

Charge-Gradient Hydrogels Enable Direct Zero Liquid Discharge for Hypersaline Wastewater Management

Wenke Xie, Jiangjiang Duan,* Jia Li, Bei Qi, Rong Liu, Boyang Yu, Hui Wang, Xinyan Zhuang, Ming Xu, and Jun Zhou*

Zero liquid discharge (ZLD), which maximizes water recovery and eliminates environmental impact, is an urgent wastewater management strategy for alleviating freshwater shortage. However, because of the high concentration of salts and broad-spectrum foulants in wastewater, a huge challenge for ZLD is lack of a robust membrane-based desalination technology that enables direct wastewater recovery without costly pretreatment processes. Here, a paradigm-shift membrane distillation (MD) strategy is presented, wherein the traditional hydrophobic porous membrane is replaced with a hydrophilic nonporous charge-gradient hydrogel (CGH) membrane that possesses hypersaline tolerance, fouling/scaling-free properties, and negligible vapor transfer resistance inside the membrane, simultaneously. Therefore, the CGH-based MD with high water flux enables direct desalination of hypersaline wastewater (130 g L^{-1}) containing broad-spectrum foulants (500 mg L^{-1}) during continuous long-term operation (200 h), and this technology paves a promising way to direct ZLD for wastewater management.

1. Introduction

More than 4 billion people worldwide suffer from freshwater shortage caused by population growth and industrialization.^[1,2] Desalination of seawater and brackish water provides a solution to alleviate freshwater shortage, however, which produces a large volume of concentrated wastewater as byproduct.^[3,4] On the other hand, industrial processes, such as shale gas production, consume substantial amounts of freshwater while producing vast quantities of hypersaline wastewater.^[5] This wastewater, if discharged to environment directly, will cause severe pollution that adversely impacts aquatic ecosystems and public health.^[6] Thus, an ambitious wastewater management

strategy of maximizing water recovery to achieve zero liquid discharge (ZLD) is pursued in the past decade.^[7,8]

Since high concentration of salts ($>100 \text{ g L}^{-1}$) and broad-spectrum foulants ($>100 \text{ mg L}^{-1}$) including surfactants, oils, and scaling agents are accumulated in wastewater,^[9,10] traditional desalination technologies hardly treat this hypersaline wastewater directly. In early ZLD systems, the wastewater firstly undergoes pretreatment processes including softening, coagulation, filtration, pH adjustment, and degasification, and then is evaporated in a brine concentrator followed by a brine crystallizer or an evaporation pond.^[11,12] Such systems hold advantages for different wastewater treatment, however, require considerable energy and capital due to the complex implements and large land footprint.

Recently, solar-driven interfacial evaporation has been proved that may be a low-cost ZLD strategy for direct hypersaline wastewater desalination.^[7,13,14] However, the water production rate of solar-driven interfacial evaporation is limited by the low and fluctuant energy density of solar irradiation.

Alternatively, membrane-based technologies enable compact and low-cost desalination with high water production rate.^[15,16] However, current membrane-based desalination technologies are still unable to direct ZLD due to their inferior hypersaline tolerance and antifouling/antiscaling performances.^[8] Reverse osmosis (RO), an efficiently membrane-based technology accounting for over 60% of the global desalination capacity, is not capable of treating high-salinity brines ($>70 \text{ g L}^{-1}$) because the osmotic pressure of such wastewaters is far beyond the limit of RO.^[9,17] Membrane distillation (MD), a membrane-based thermal separation process utilizing low-grade heat, possesses high tolerance of salinity but high risk of fouling and scaling.^[18–20] In a traditional MD system, hot brine and cold purified water are separated by a hydrophobic porous membrane, which allows water vapor transmembrane transport driven by a vapor pressure difference but blocks liquid and solute transport. However, foulants with a trace concentration ($<1 \text{ mg L}^{-1}$) can cause wetting of the hydrophobic porous membrane, which ultimately lead to desalination process failure of MD.^[21–24] Although the wetting resistance of MD membranes for one type of organic foulants can be improved by interfacial and porous structural engineering approaches,^[25–28] the design of a broad-spectrum antiwetting membrane is still elusive.

W. Xie, Dr. J. Duan, Dr. J. Li, B. Qi, R. Liu, B. Yu, H. Wang, X. Zhuang, Prof. J. Zhou
Wuhan National Laboratory for Optoelectronics
Huazhong University of Science and Technology
Wuhan 430074, China
E-mail: jiangjduan@hust.edu.cn; jun.zhou@mail.hust.edu.cn
Prof. M. Xu
School of Materials Science and Engineering
Huazhong University of Science and Technology
Wuhan 430074, China

 The ORCID identification number(s) for the author(s) of this article can be found under <https://doi.org/10.1002/adma.202100141>.

DOI: 10.1002/adma.202100141

Herein, we propose a paradigm-shift MD strategy of replacing traditional hydrophobic porous membrane with a charge-gradient hydrogel (CGH) membrane, which enables direct and ultrastable ZLD for wastewater management. The CGH membrane features the gradient distribution of charged groups on its cross section, which induces the gradient of free water content and osmotic pressure that enables high water flux and salt rejection. Although the charged hydrogels with multi-layer structures have been used for forward osmosis desalination as draw agents,^[29] their structures and functions are different from the CGH membranes with single-layer structures. Compared with a hydrophobic porous membrane, our CGH membrane is hydrophilic and nonporous, and possesses simultaneous hypersaline tolerance and fouling/scaling-free performances. In addition, the CGH with negligible vapor diffusion resistance inside the membrane achieves $\approx 110\%$ maximized enhancement in water flux compared with commercial hydrophobic membranes. Furthermore, our CGH membrane enables stable desalination of high-salinity wastewater (130 g L^{-1}) containing broad-spectrum foulants (500 mg L^{-1}) during continuous long-term operation for 200 h.

2. Results and Discussions

2.1. Merits of Charge-Gradient-Hydrogel-Based Membrane Distillation

Hydrogels are 3D polymeric networks with water as the dispersed medium,^[30,31] which provide a material platform for the manufacture of innovative MD membranes because of the unique state of water in hydrogels.^[32,33] Typically, water molecules in hydrogels are confined in polymeric networks with mesh size of $\approx 10 \text{ nm}$,^[34,35] and possess significantly different hydrodynamic properties from those of bulk water.^[36–38] The hydrodynamic behaviors of liquid water are based on the classical continuum model, while water in hydrogels is discontinuous due to a combination of hydrodynamic drag and obstruction effects of the macromolecular chains.^[39] Therefore,

water in hydrogels is not in the state of a liquid, and hydrogels are considered to be the quasi-solid materials. As shown in **Figure 1**, different from hydrophobic porous membrane blocking liquid brine penetration based on interfacial antiwetting mechanism, CGH blocking liquid brine penetration is based on the molecule confinement effect. Namely, liquid brine can't penetrate the quasi-solid hydrogels, while water molecules in the hydrogel surface can diffuse and evaporate freely. Therefore, our CGH enables desalination with a low fouling risk for wastewater treatment. Moreover, a serious salt accumulation occurs at the vapor surface for hydrophobic porous membranes due to concentration polarization effect. On the contrary, hydrogels containing charged groups have strong salt-rejection effect because of their inherently high osmotic pressure ranging from several to hundreds bar based on the charged polymer concentration.^[40] Hence, CGH with a high osmotic pressure possesses robust hypersaline tolerance and antiscaling property. In addition, evaporation, in traditional MD, occurs at the interface between hot brine and hydrophobic membrane, thus there is a large transfer resistance for vapor diffusing in tortuous nanopores.^[9,41] In comparison, evaporation in CGH-based MD occurs at the surface of the hydrogel membrane in the permeate side, so the vapor diffusion resistance in the hydrogel membrane is eliminated (see Note S5, Supporting Information). As a result, the CGH shows a high water flux. Overall, our CGH-based MD has several advantages, including: (1) low vapor transfer resistance because of vapor diffusion in free space rather than nanopores; (2) fouling-free because of the nonliquid state of CGHs; and (3) scaling-free due to the strong salt-rejection effect of CGHs.

2.2. High Water Flux in Charge-Gradient Hydrogels

We have developed a diffusion-assisted copolymerization method to prepare CGH (Figure S1, Supporting Information). **Figure 2b** demonstrates a roll of CGH membrane with a length of 500 cm and a width of 10 cm using this preparation method, thereby indicating the scalability of the CGH. On the

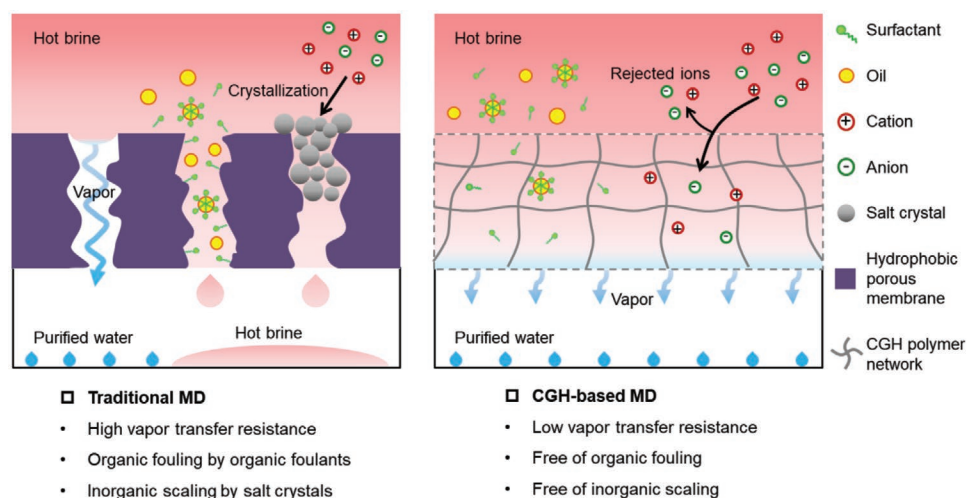


Figure 1. Comparison of traditional MD and CGH-based MD. Traditional MD with a hydrophobic porous membrane has high vapor transfer resistance and fouling/scaling tendency. CGH-based MD has low vapor transfer resistance and is free of fouling and scaling.

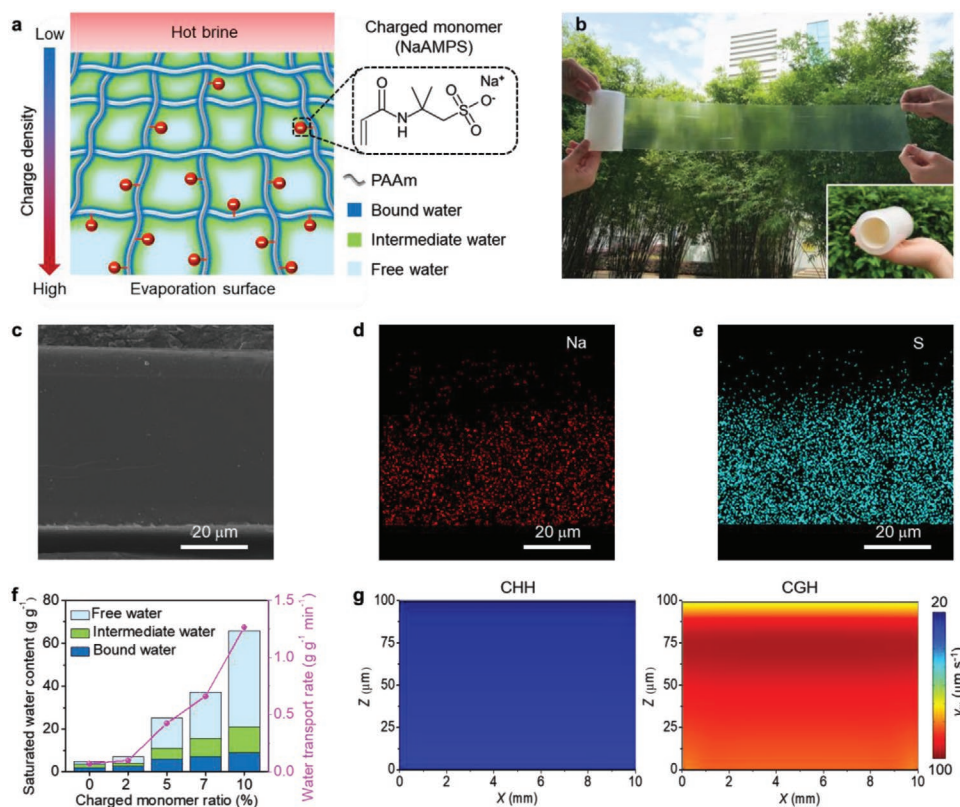


Figure 2. Charge-gradient structures and water transport performances of CGH. a) Schematic of the section structure of CGH. Charged monomers (NaAMPS) with a gradient distribution are copolymerized with the neutral monomers (AAm), and the included water exists as three types, that is, bound water, intermediate water and free water, according to the interaction between water molecules and polymer chains. b) Photograph of a roll of CGH membrane (500 cm by 15 cm). c) Cross-section SEM image of the dried CGH and d,e) corresponding EDS mapping of sodium (Na, red) (d) and sulfur (S, blue) (e), which represent the gradient distribution of NaAMPS in the polymer skeleton of CGH. f) Water state and transport rate of CHH with different charged monomer ratios. The water state is investigated by DSC (Note S1, Supporting Information), and the water transport rate is calculated using swelling experiments (Note S2, Supporting Information). g) Simulation of water transport speed in a CHH (left) and CGH (right) membrane with the same charged monomer ratio.

cross section of the CGH membrane, the charged monomer (sodium-2-acrylamido-2-methylpropane-1-sulfonate, NaAMPS) had a gradient distribution in a neutral polyacrylamide (PAAm) skeleton (Figure 2a,c–e). Compared with a hydrophobic porous poly(tetrafluoroethylene) (PTFE) membrane (Figure S2a,b, Supporting Information), a CGH membrane is hydrophilic and nonporous (Figure S2c, d, Supporting Information).

For the CGH-based MD, water evaporation occurs at the permeate side rather than the feed side of traditional MD. During the desalination/distillation process, water and heat transported from a hot feed across the CGH membrane to the evaporation surface; thus, high water and heat transport speeds are essential to achieve high vapor flux. According to the strength of the interaction between the water molecules and the polymer chains, water in a hydrogel can be classified into three types: bound water (strong interaction), intermediate water (medium interaction), and free water (weak interaction).^[42,43] Among them, free water makes the greatest contribution to water molecules and heat transport.^[44,45] Charged hydrogels have weak interactions between polymer chains due to electrostatic repulsion;^[46] therefore, they are highly swollen and are expected to contain a high proportion of free water. To confirm this viewpoint, we prepared a series of charge-homogeneous hydrogels

(CHHs) with different charged monomer ratios. Then their water states and water transport rates were investigated by differential scanning calorimetry (DSC) (Figure S3a and Table S1, Supporting Information) and dynamic analysis of swelling process (Figure S3b,c, Supporting Information), respectively. As the charged monomer ratio increased from 0% to 10%, the free water content (1.38–44.92 g g⁻¹) in the CHHs and the water transport rate (0.07–1.27 g g⁻¹ min⁻¹) significantly increased (Figure 2f). In addition, the thermal conductivity of the CHHs also increased from 0.49 to 0.66 W m⁻¹ K⁻¹ with the increase of the charged monomer ratio (Figure S3d, Supporting Information). However, the mechanical strength of the CHHs significantly decreased from 0.24 MPa to 0.01 MPa as the charged monomer ratio increased from 0% to 10% (Figure S3e,f, Supporting Information), which is unfavorable for the robustness required for vacuum MD. By contrast, the CGH membrane was robust and had 10–50% higher mechanical strength than CHH membranes at the same charge ratio (Figure S4, Supporting Information).

In addition, the charge gradient in the hydrogel formed an osmotic pressure gradient, which pumped water from the low charge density side to the high charge density side. Using COMSOL simulation of the charged hydrogel swelling in the

MD system (Note S4, Supporting Information), we found that the water transport speed in the CGH ($\approx 80\text{--}95 \mu\text{m s}^{-1}$) was significantly higher than that in the CHH ($\approx 18\text{--}24 \mu\text{m s}^{-1}$) (Figure 2g). This is caused by the osmotic pressure pumping effect and the higher free water content close to the evaporation side. Furthermore, if the charge gradient was reversed (denoted as R-CGH), the osmotic pressure gradient was also reversed, thus, increased the resistance for water transport in the R-CGH. As a result, the water transport speed in the R-CGH ($\approx 1.6\text{--}2.4 \mu\text{m s}^{-1}$) was much lower than that in the CHH and CGH (Figure S5, Supporting Information). Therefore, CGH achieves a simultaneous high water/heat transport speed due to its charge and free water gradients from the feed side to the evaporation side.

Then, we tested the water evaporation flux of the charged hydrogels (including CGH and CHH) and commercial PTFE membranes using a standard vacuum MD device (Figure 3a). The feed solution was the artificial seawater (35 g L^{-1} NaCl solution). Under the operating condition of feed temperature of $60 \text{ }^\circ\text{C}$, permeate pressure of 3 kPa , and feed flow rate of 7.12 L h^{-1} (If not specified, the experiments of vacuum MD were conducted in this operation condition), the water flux of CGH membranes with thickness of $200 \mu\text{m}$ increased from 12.51 to $14.01 \text{ L m}^{-2} \text{ h}^{-1}$ as the charged monomer ratio increased from 1% to 4% , and was significantly higher than the water flux of PTFE membranes ($7.99 \text{ L m}^{-2} \text{ h}^{-1}$). In addition, the water flux of CGH was also higher than that of CHH ($11.03\text{--}13.93 \text{ L m}^{-2} \text{ h}^{-1}$)

at the same charge ratio (Figure 3b). It is worth noting that the water flux could be greatly improved in optimized experimental conditions, such as higher feed temperature, higher feed flow rate, or lower permeate pressure.

We measured the water flux of CGH (4% charged monomer ratio) and PTFE at different membrane thicknesses and feed temperatures (Figure S6, Supporting Information); and theoretically estimated the water flux by numerical simulation (Note S5, Supporting Information). The theoretical results matched very well with the experimental results. CGH exhibited $\approx 60\text{--}110\%$ enhancement in the water flux ($5.58\text{--}2773 \text{ L m}^{-2} \text{ h}^{-1}$) compared with that of PTFE ($2.65\text{--}1763 \text{ L m}^{-2} \text{ h}^{-1}$) at the membrane thicknesses of $200 \mu\text{m}$ for a wide range feed temperatures ($40\text{--}80 \text{ }^\circ\text{C}$) (Figure 3d). Note that the water flux of CGH was insensitive to the membrane thickness and maintained a high water flux ($13.86 \text{ L m}^{-2} \text{ h}^{-1}$) even at a membrane thickness of $500 \mu\text{m}$ because of its negligible vapor transfer resistance inside the membrane. By contrast, PTFE achieved a high water flux ($>10 \text{ L m}^{-2} \text{ h}^{-1}$) only when the membrane thickness was less than $100 \mu\text{m}$ (Figure 3c). Furthermore, the water flux of the CGH can be increased to $29.48 \text{ L m}^{-2} \text{ h}^{-1}$ by increasing the feed flow rate to 90 L h^{-1} (Figure S7a, Supporting Information), this is because the increase in feed flow rate suppresses the temperature polarization effect (i.e., increases the evaporation surface temperature) (Figure S7b, Supporting Information). Despite a more severe temperature polarization (lower evaporation surface temperature) of CGH due to the lack of

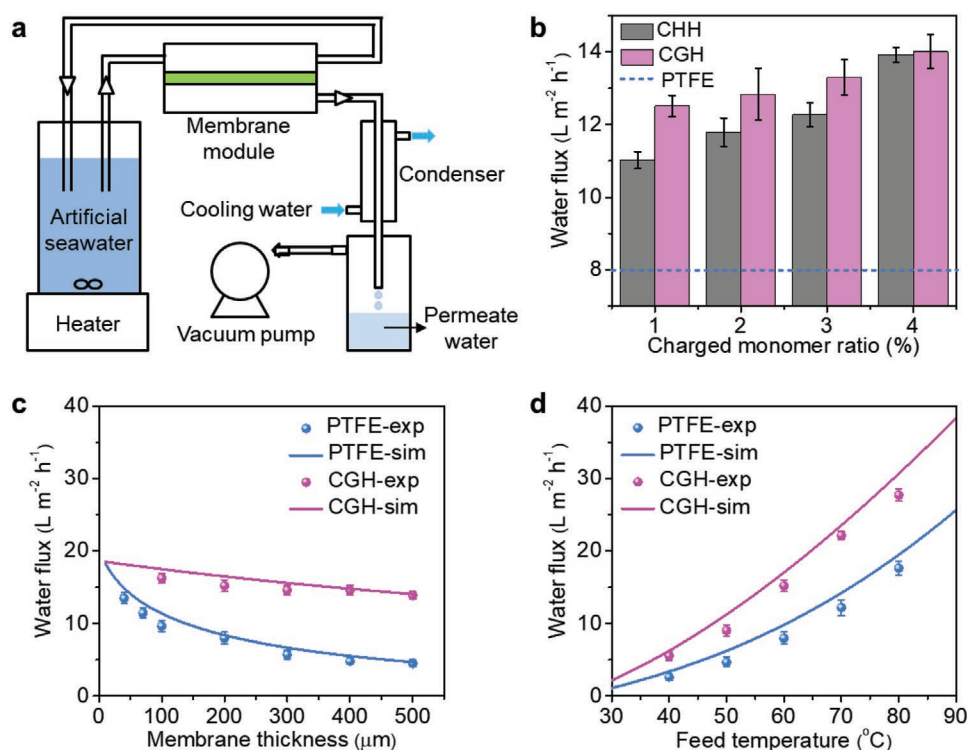


Figure 3. High flux of CGH in a vacuum MD system. a) Schematic illustration of the vacuum MD setup. b) Comparison in water flux of CHH and CGH membranes with different charged monomer ratios (membrane thickness: $200 \mu\text{m}$; feed temperature: $60 \text{ }^\circ\text{C}$). The dashed blue line represents the water flux of commercial PTFE membrane under the same condition. c, d) Water flux of PTFE and CGH membranes as a function of membrane thickness (feed temperature: $60 \text{ }^\circ\text{C}$) (c) and feed temperature (membrane thickness: $200 \mu\text{m}$) (d). The charged monomer ratio of CGH is 4% . The symbols represent experimental results, and the curves represent theoretical results. Each error bar represents the deviation from at least five data points.

hydrodynamic mixing inside the CGH, the water flux of the CGH (15.22–29.48 L m⁻² h⁻¹) was still 56–90% higher than that of the PTFE (7.99–18.90 L m⁻² h⁻¹), which was also higher than other hydrophobic porous membranes reported in literatures (Figure S7, Supporting Information). Because of the higher water flux and lower heat loss (lower average temperature of feed solution) (Table S2, Supporting Information), the energy efficiency (represented by gain output ratio) of the CGH membrane was 0.83–0.95 at the feed temperatures of 40–80 °C, which was 7–16% higher than that of the PTFE membrane. Accordingly, the CGH membrane showed 6–14% lower energy consumption than PTFE membrane (Figure S8, Supporting Information). Moreover, in the air-gap MD where the vapor transport resistance is dominated by the air gap, our CGH membrane still exhibited 37–70% enhancement in water flux compared with that of PTFE membrane (Figure S9, Supporting Information). In addition, the good desalination performances of our CGH-based MD could be achieved in a large-scale device in practical application by optimizing the configurations and operation conditions, for example, smaller hydraulic diameters and higher feed flow rates.

2.3. Resistance to Organic Fouling

Natural seawater and industrial wastewater contain various organic foulants, such as oils and surfactants, which can cause organic fouling of membranes. It is worth noting that the fouling mechanism caused by oils and surfactants is different. Oils induce pore blockage for vapor transport, while surfactants only induce pore wetting. Despite different fouling mechanisms, oils and surfactants will both cause the decline of hydrophobicity of membranes, and ultimately induce the failure of

MD desalination. We selected four typical foulants as representatives, that is, sodium dodecyl benzene sulfonate (SDBS, hydrophilic surfactant), Span-80 (hydrophobic surfactant), corn oil, and liquid paraffin, to investigate the organic fouling resistance of PTFE and CGH.

Liquid entry pressure (LEP), the minimum pressure to press liquid into the membrane pores,^[47] is often used to evaluate the wetting resistance of hydrophobic porous membranes. In this study, we used this parameter to characterize the fouling resistance of the PTFE and CGH membranes. As shown in Figure 4a, when the first water droplet dropped, the corresponding pressure was considered to be the LEP. The hydrophobic porous PTFE membrane was sensitive to organic foulants. Its LEP significantly decreased from ≈2375 kPa to below 10 kPa (Figure 4d) and became less hydrophobic after pollution (Figure S10a, Supporting Information). When pressure (53.5 kPa) was applied over the LEP of a polluted PTFE membrane, continuous water moved across the PTFE membrane, which was indicated by the visual color change of CuSO₄ from white to blue (Figure 4b). For CGH membrane, although the water molecules can enter the hydrophilic CGH, no water droplet dropped even at a high pressure of 697 kPa (Figure 4c) due to the no fluid-state water in CGH. Moreover, the CGH membrane showed no obvious changes in its LEP value (Figure 4d) and hydrophilicity (Figure S10b, Supporting Information) before and after pollution. These results indicate excellent fouling resistance of our CGH membrane.

We further evaluated the organic fouling resistance of CGH membrane and PTFE membrane in vacuum MD by monitoring the water flux and permeate ionic conductivity when treating artificial seawater (35 g L⁻¹ NaCl solution) containing 10 mg L⁻¹ organic foulant. The water fluxes of CGH membranes were stable over the entire desalination run, with nearly 99.9% salt

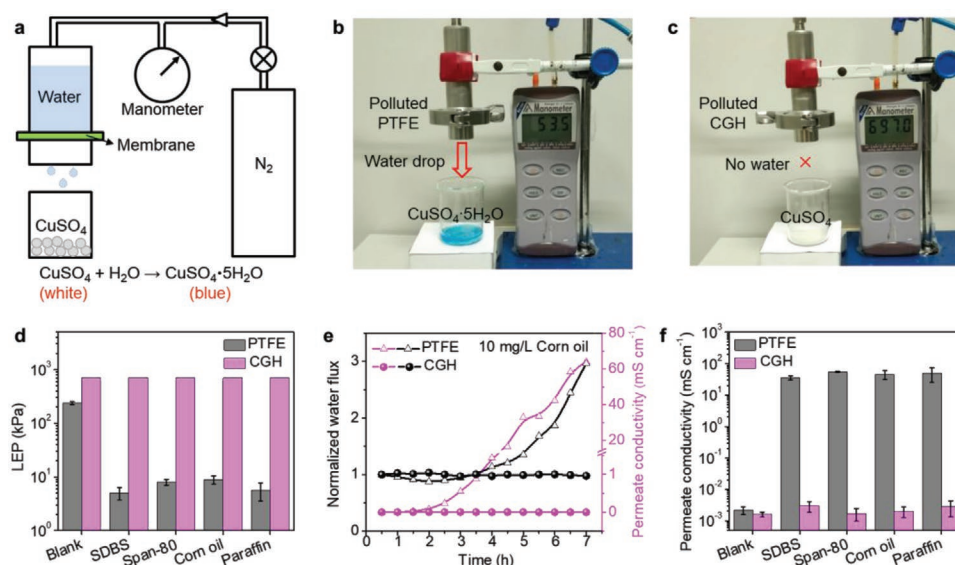


Figure 4. Resistance to organic fouling of CGH. a) Schematic illustration of the LEP measuring device. b,c) Photograph of the LEP measurement for a PTFE membrane (b) and a CGH membrane (c) polluted by corn oil. d) LEP values of the PTFE and CGH membranes before and after they were polluted by different organic foulants. e) Normalized water flux and permeate ionic conductivity of PTFE and CGH membranes in the vacuum MD process. The feed solution was artificial seawater (35 g L⁻¹ NaCl solution) containing 10 mg L⁻¹ corn oil. f) Permeate ionic conductivity of PTFE and CGH membranes after treating artificial seawater containing different organic foulants (10 mg L⁻¹) for 10 h. Standard deviations indicated by the error bars are the results of five experiments.

rejection, and the corresponding permeate conductivities were maintained below $5 \mu\text{S cm}^{-1}$ (Figure 4e,f, and Figure S10c–e, Supporting Information). In comparison, the PTFE membranes completely lost their desalination ability after continuous operation indicated by dramatically increase in permeate conductivity (Figure 4f). For the cases of oils (corn oil and liquid paraffin) as foulants, the water flux of PTFE membrane firstly decreased slightly due to pore blockage and then increased greatly due to pore wetting (Figure 4e, and Figure S10c, Supporting Information). For the cases of surfactants (SDBS and span-80) as foulants, the water flux increased significantly within one hour caused by pore wetting (Figure S10d,e, Supporting Information). These results suggest our CGH membrane has more robust fouling resistance compared with PTFE membrane.

2.4. Antiscaling Property

In addition to organic fouling, inorganic scaling is another challenge for MD treatment of high-salinity wastewater. To

evaluate the resistance to scaling of CGH membrane, we conducted a continuous concentration experiment using a 35 g L^{-1} NaCl solution as initial feed solution (Figure 5a). The concentration factor represents the degree of concentration, which is defined as the ratio of concentrate concentration to initial concentration.^[24] The water flux of PTFE membrane ($8.74\text{--}3.35 \text{ L m}^{-2} \text{ h}^{-1}$) decreased faster than that of CGH membrane ($13.31\text{--}10.78 \text{ L m}^{-2} \text{ h}^{-1}$) before concentration factor was less than 3 because salt crystals blocked the membrane pores; and then slightly increased to $4.28 \text{ L m}^{-2} \text{ h}^{-1}$ when concentration factor was higher than 3. Moreover, the permeate ionic conductivity of PTFE membrane dramatically increased from 8.0 to 195.4 mS cm^{-1} when concentration factor was higher than 3, which indicated that the PTFE membrane was wetted because of scaling. The scaling phenomenon was directly observed on the permeate cell (Figure S11a, Supporting Information) and PTFE membrane (Figure S11b,c, Supporting Information). For CGH membrane, the water flux linearly decreased ($13.81\text{--}3.51 \text{ L m}^{-2} \text{ h}^{-1}$) with the increase of concentration factor when the concentration factor is less than 8.69. This is because

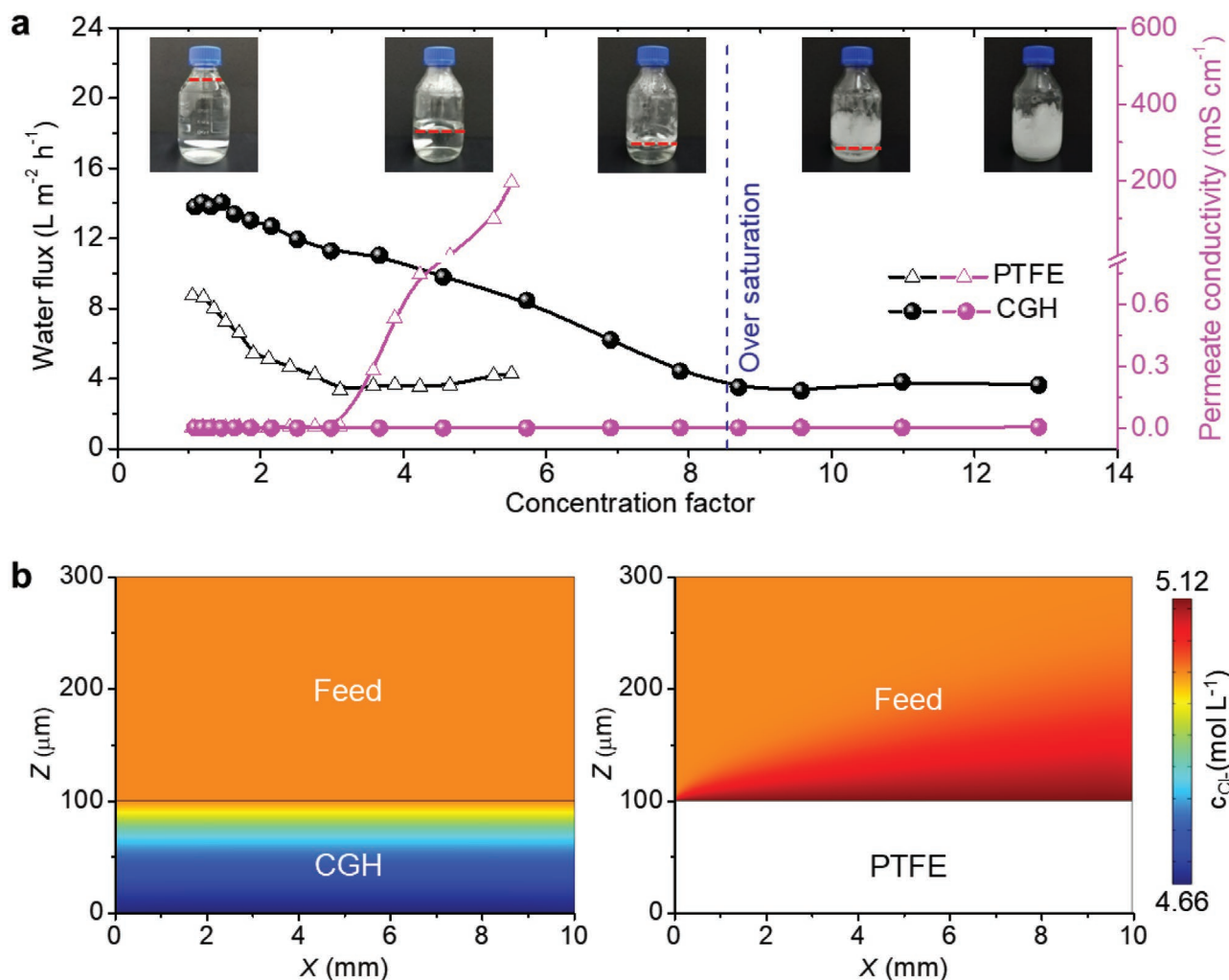


Figure 5. Resistance to inorganic scaling of CGH. a) Variations in water flux and permeate ionic conductivity versus concentration factor during continuous concentration of artificial seawater via vacuum MD. Insets: Concentration-factor-dependent photographs of the feed solution in the CGH-based MD process. b) Simulated chloride ion (Cl^-) concentration profiles for the CGH-based MD (left) and PTFE-based MD (right) using COMSOL software, further explaining the salt rejection of the CGH.

the increase in feed concentration (0.6–5.2 mol L⁻¹) reduces the saturated vapor pressure (4.42–3.43 kPa) on the evaporation surface of CGH membrane (Figure S12a, Supporting Information) caused by the decrease in water molar fraction (95.9–72.4%) (Figure S12b, Supporting Information). When the concentration factor was higher than 8.69, the NaCl in the feed solution reached saturation (\approx 5.2 mol L⁻¹), and a stable water flux for CGH membrane was maintained. It is worth noting that the permeate ionic conductivity for CGH membrane maintained at a low values of \approx 1.37–4.33 μ S cm⁻¹ throughout the whole concentration experiment until water and solute were completely separated (see photographs in Figure 5a); that is, our CGH membrane enabled ZLD. In addition, no salt crystals were observed on either the permeating cell (Figure S11d, Supporting Information) or CGH membrane surface (Figure S11e,f, Supporting Information) after disconnecting the membrane module. These results prove that our CGH membrane has excellent antiscaling performance.

The antiscaling performance of the CGH is attributed to its inherently high osmotic pressure of 174–245 bar (Figure S13a, Supporting Information), which was much higher than that of feed solution (15–122 bar) (Figure S13b, Supporting Information). Because of the high osmotic pressure, the CGH dramatically draws water but rejects about 10–30% salt from the feed solution (Figure S14b, Supporting Information) until its osmotic pressure is equal to that of feed solution, which is similar as the forward osmosis desalination. As a result, at the swelling equilibrium state, the water fraction of CGH membrane (72.4–95.9%) was similar with that of feed solution (76.4–97.3%) (Figure S12b, Supporting Information), while the salt concentration in CGH membrane (0.43–4.59 mol L⁻¹) was lower than the salt concentration in feed solution (0.6–5.0 mol L⁻¹) (Figure S14a, Supporting Information). To further prove the antiscaling mechanism, we simulated the ions profiles in hydrogel-based MD using COMSOL simulation of the charged hydrogel swelling (Note S4, Supporting Information). Due to the gradient distribution of charged groups ($-\text{SO}_3^-$) in the CGH (0–0.8 mol L⁻¹) (Figure S15a, left, Supporting Information), the concentration of chloride ions (Cl^-) gradually decreased from 5.0 to 4.66 mol L⁻¹ from the feed side to the evaporation surface (Figure 5b, left, and Figure S15b, left, Supporting Information), which was lower than that of feed solution (saturated NaCl solution, \approx 5.0 mol L⁻¹). Even though more sodium ions (Na^+) existed in CGH for the conservation of charge (Figure S15c, left, Supporting Information), some of them are trapped by the $-\text{SO}_3^-$ groups in the polymer network, whose concentration is equal to that of $-\text{SO}_3^-$. And the concentration of mobile Na^+ that can form salt crystals was equal to the concentration of Cl^- ; hence, it is difficult to form salt crystals in the CGH membrane. Note that the CHH and R-CGH also exhibited salt-rejection effect, while the antiscaling performance of CGH was more prominent than that of CHH and R-CGH because of the lower NaCl concentration on the evaporation surface of the CGH (Figure S15, Supporting Information). By contrast, the ions profiles in PTFE-based MD were also calculated by the COMSOL simulation (Note S7, Supporting Information). Due to the concentration polarization effect induced by interfacial evaporation, the concentration of Cl^- (equal to the concentration of Na^+) at the evaporation surface exceeded

that in the feed solution (Figure 5b, right); therefore, scaling is inevitable in the PTFE membrane for high-salinity wastewater treatment.

2.5. Long-Term Stability

The durability of membranes is important for the viability of ZLD. To evaluate the long-term stability of CGH-based MD, an artificial wastewater containing high concentration of salts (130 g L⁻¹) and broad-spectrum foulants (500 mg L⁻¹) was continuously treated for 200 h. The wastewater is composed of various inorganic salts and organic foulants, including NaCl (100 g L⁻¹), KCl (3.03 g L⁻¹), MgSO₄ (8.73 g L⁻¹), MgCl₂ (13.56 g L⁻¹), CaSO₄ (5.4 g L⁻¹), humic acid (HA, 100 mg L⁻¹), SDBS (100 mg L⁻¹), Span-80 (100 mg L⁻¹), corn oil (100 mg L⁻¹), and liquid paraffin (100 mg L⁻¹) (inset in Figure 6a). Thanks to the robust performances of our CGH membrane, its water flux (9.14–10.58 L m⁻² h⁻¹) and permeate ionic conductivity (0.95–3.94 μ S cm⁻¹) were stable over 200 h (Figure 6a). The slight reduction in the water flux was attributed to the increase in the condenser temperature which can be avoided in practical application. The water quality was directly measured using a conductivity meter, and the ionic conductivity of the wastewater and purified water were 108.9 mS cm⁻¹ and 1.676 μ S cm⁻¹, respectively (Figure 6b), which indicates the effective purification of the wastewater. The concentrations of primary ions (Na^+ , Mg^{2+} , K^+ , and Ca^{2+}) in the wastewater were significantly reduced by \approx 4–5 orders of magnitude after desalination (Figure 6c), which meets the World Health Organization (WHO) standard for drinking water. Furthermore, we used Raman spectroscopy to analyze the organic components in purified water. No characteristic peaks for organic compounds were found in the Raman spectra of purified water (Figure 6d), which confirms the absence of organic contaminants. Furthermore, our CGH enabled stable desalination of the real wastewater produced from RO desalination process (Figure S16, Supporting Information), indicating the feasibility for practical applications. In addition, the desalination performance of the CGH membrane was stable during five deswelling-swelling cycles treatment (Figure S17, Supporting Information), demonstrating the excellent reusability.

3. Conclusion

We report a CGH membrane with high water flux, and excellent fouling/scaling-free properties, which is a promising alternative for MD to treat hypersaline wastewater. The high water flux is attributed to the small vapor transfer resistance on the evaporation surface and high water/heat transport speed in the CGH matrix. The fouling-free and scaling-free properties are attributed to the inherent quasi-solid state and high osmotic pressure of charged hydrogels. Because of these merits, CGH-based MD is capable of ZLD for wastewater management, for example, from RO desalination plants and shale gas extraction. In addition, we propose that the water flux of the CGH membrane can be further enhanced by designing a 3D topographic evaporation surface^[48] and eliminating temperature polarization.^[18]

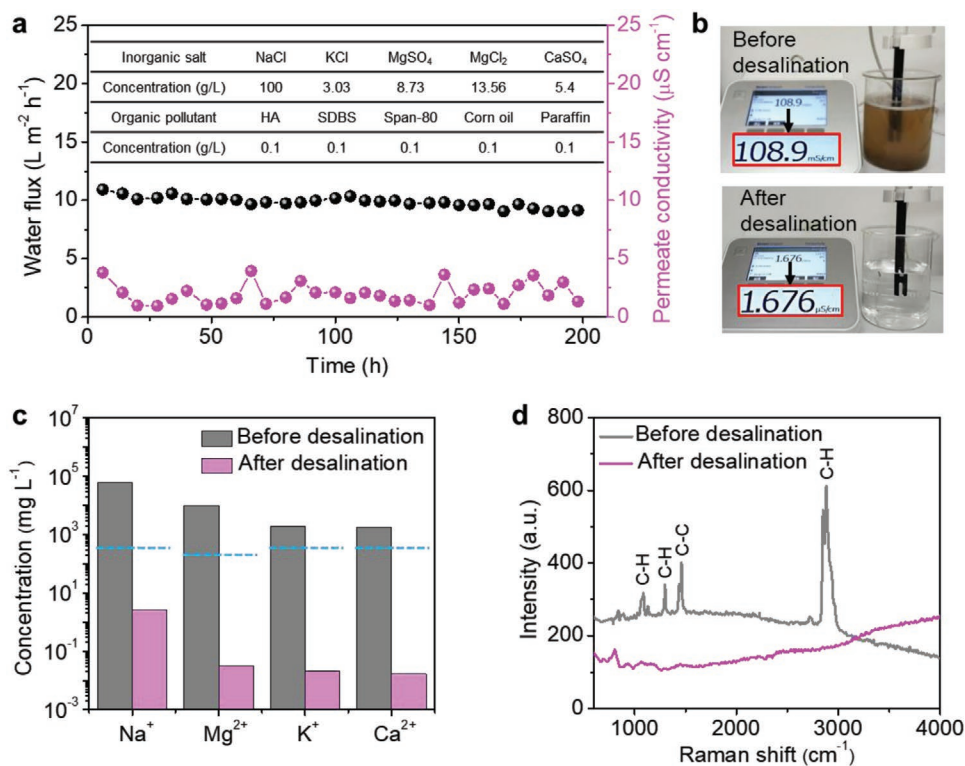


Figure 6. Long-term stability and desalination performance of CGH. a) Water flux and permeate ionic conductivity of CGH-based MD during continuous desalination of high-salinity wastewater consisting of various inorganic salts and organic foulants. Inset: Chemical component of the initial wastewater. b) Photographs of the wastewater and corresponding ionic conductivity before and after desalination. The ionic conductivity units of the wastewater before and after desalination are mS cm⁻¹ and μS cm⁻¹, respectively. c) Measured concentrations of four primary cations in the wastewater before and after desalination. The dashed blue lines refer to the WHO standards of concentration for drinking water. d) Raman spectra of the wastewater before and after desalination.

4. Experimental Section

Chemicals and Materials: 2-Acrylamido-2-methyl-1-propanesulfonic acid sodium salt (NaAMPS) as charged monomer, acrylamide (AAM) as neutral monomer, *N,N'*-methylenebis (acrylamide) (MBAA) as cross-linking agent and 2-hydroxy-4'-(2-hydroxyethoxy)-2-methylpropiophenone as UV initiator were purchased from Sigma-Aldrich. Agarose (biochemical reagent), sodium dodecyl benzene sulfonate (SDBS), Span-80, liquid paraffin, NaCl, KCl, MgSO₄, MgCl₂, CaSO₄, and humic acid (HA) were purchased from Sinopharm Chemical Reagent Co., Ltd. The PTFE membranes were commercial products purchased from Hongfu Co., Ltd. Milli-Q (18.3 MΩ) water was used in all experiments.

Preparation of the Charge-Gradient Hydrogels: The charged monomer solution contained 3 mol L⁻¹ monomer NaAMPS/AAM (with different molar ratios), 2 wt% agarose with respect to the weight of the solution, 0.05 mol% MBAA, and 0.1 mol% 2-hydroxy-4'-(2-hydroxyethoxy)-2-methylpropiophenone with respect to the monomer. The solution was heated at 95 °C for 20 min to obtain a transparent pre-hydrogel solution. The hot solution was sealed into a glass mold and then cooled at room temperature for 30 min, thereby ensuring complete gelling of the agarose. The neutral pre-hydrogel was synthesized using AAM as monomer using the same process as that for the charged pre-hydrogel. Next, the two pre-hydrogels were placed in contacted in a sealed glass container, and the container was subsequently irradiated with 365 nm ultraviolet light (≈4 mW cm⁻²) for 4 h to obtain CGH. In the polymerization process, the charged monomer NaAMPS simultaneously diffused and was polymerized to form a CGH membrane. A schematic illustration of the CGH fabrication procedure was shown in Figure S1 (Supporting Information).

Preparation of the Charge-Homogeneous Hydrogels: The monomer solution of CHH was the same as that of CGH. The solution was heated

at 95 °C for 20 min to obtain a transparent pre-hydrogel solution. The hot solution was sealed into a glass mold and then cooled at room temperature for 30 min, thereby ensuring complete gelling of the agarose. Next, the glass mold which was filled with pre-hydrogel was irradiated under a 365 nm ultraviolet light (≈4 mW cm⁻²) for 4 h to obtain the CHH.

Vacuum Membrane Distillation Experiments: In the vacuum MD setup, a membrane with effective membrane area of 33.18 cm² (diameter, 65 mm) was mounted between two chambers. One serves as feed side was filled with flowing hot feed solution (height, 9.5 mm), and the other serves as permeate side was connected to a vacuum pump (YUHUA, SHZ-958) through a condenser. The feed solution was heated and stirred in a water bath, and then pumped through the membrane module at a flow rate of 7.12 L h⁻¹ (equivalent to a cross flow velocity of 6.406 mm s⁻¹). Water vapor was condensed by a cooling water condenser (20 °C). The permeate pressure was controlled at ≈3 kPa. The water flux was calculated by measuring the volume of permeate water, and salt rejection was evaluated by measuring the conductivity of permeate water using a conductivity meter (Mettler Toledo, S-230). The feed solutions in vacuum MD experiments were prepared as follows: Firstly, the inorganic salts of different masses were dissolved in pure water. Then the organic foulants were added to the solutions and they were stirred at 1000 r min⁻¹ for 6 h to obtain uniformly dispersed feed solutions.

Air-Gap Membrane Distillation Experiments: The air-gap MD setup has the same feed side with the vacuum MD setup. Its permeate side is an air gap of 2 mm and a condense layer which was connected to flowing cooling water of 20 °C. To prevent the water of hydrogel membrane from contaminating the product water, it was tilted the membrane device at about 40° so that the evaporated water could flow out of the prototype as soon as it condenses on the condenser.

Liquid Entry Pressure Measurements: The measured membrane was sandwiched between two stainless-steel cells. The top cell (feed side) was filled with water and connected with a compressed gas cylinder. The pressure of the feed side slowly increased at a 5 kPa interval during the measurement. At each pressure interval, the membrane was kept at a constant pressure for 10 min. When the first water droplet dropped, the corresponding pressure was considered to be the LEP. For convenient observation, white anhydrous CuSO₄ powder was used as an indicator of water. When there is a water droplet from the membrane, white CuSO₄ changes into blue CuSO₄·5H₂O.

Characterizations: The morphology of the wetted CGH surface was observed using an environmental scanning electron microscope (FEI, Quanta 200). The cross-section of the dried CGH was observed using a scanning electron microscope (FEI, Nova Nano SEM 450). The elemental distributions of the dried CGH were analyzed using energy-dispersive X-ray mapping in SEM. Before this test, the CGH was snapped in liquid nitrogen and then dried. Optical microscopy images were obtained using an optical microscope (Nikon, LV-LH50PC). The mechanical properties were determined by tensile tests using a universal mechanical test machine (REGER, RGM-4005T). The water state in the CHH was observed using a differential scanning calorimeter (Perkin Elmer, Diamond DSC). The ionic conductivity of the water samples was measured using a conductivity meter (Mettler Toledo, S-230). The concentration of ions was tracked using ICP-OES (Leeman Labs, Prodigy Plus). The organic foulants in permeate water were characterized using a laser confocal Raman spectrometer (Horiba JobinVvon, LabRAM HR800) with a He–Ne laser ($\lambda = 532$ nm).

Supporting Information

Supporting Information is available from the Wiley Online Library or from the author.

Acknowledgements

This work was supported by the National Natural Science Foundation of China (51872101, 52002139), the National Program for Support of Topnotch Young Professionals (52025027), the program for HUST Academic Frontier Youth Team (2017QYTD11) and Director Fund of WNLO. The authors thank the Center for Nanoscale Characterization & Devices, WNLO-HUST and the Analysis and Testing Center of Huazhong University of Science and Technology for their support.

Conflict of Interest

The authors declare no conflict of interest.

Data Availability Statement

The data that support the findings of this study are available from the corresponding author upon reasonable request.

Keywords

charge-gradient hydrogels, desalination, membrane distillation, wastewater management, zero liquid discharge

Received: January 7, 2021

Revised: February 18, 2021

Published online:

- [1] C. J. Vorosmarty, P. B. McIntyre, M. O. Gessner, D. Dudgeon, A. Prusevich, P. Green, S. Glidden, S. E. Bunn, C. A. Sullivan, C. R. Liermann, P. M. Davies, *Nature* **2010**, 467, 555.
- [2] S. B. Grant, J. D. Saphores, D. L. Feldman, A. J. Hamilton, T. D. Fletcher, P. L. Cook, M. Stewardson, B. F. Sanders, L. A. Levin, R. F. Ambrose, A. Deletic, R. Brown, S. C. Jiang, D. Rosso, W. J. Cooper, I. Marusic, *Science* **2012**, 337, 681.
- [3] M. Elimelech, W. A. Phillip, *Science* **2011**, 333, 712.
- [4] J. R. Werber, C. O. Osuji, M. Elimelech, *Nat. Rev. Mater.* **2016**, 1, 16018.
- [5] C. Boo, J. Lee, M. Elimelech, *Environ. Sci. Technol.* **2016**, 50, 12275.
- [6] L. F. Greenlee, D. F. Lawler, B. D. Freeman, B. Marrot, P. Moulin, *Water Res.* **2009**, 43, 2317.
- [7] N. Xu, J. Li, Y. Wang, C. Fang, X. Li, Y. Wang, L. Zhou, B. Zhu, Z. Wu, S. Zhu, J. Zhu, *Sci. Adv.* **2019**, 5, 7013.
- [8] T. Tong, M. Elimelech, *Environ. Sci. Technol.* **2016**, 50, 6846.
- [9] A. Deshmukh, C. Boo, V. Karanikola, S. Lin, A. P. Straub, T. Tong, D. M. Warsinger, M. Elimelech, *Energy Environ. Sci.* **2018**, 11, 1177.
- [10] J. Lee, C. Boo, W.-H. Ryu, A. D. Taylor, M. Elimelech, *ACS Appl. Mater. Interfaces* **2016**, 8, 11154.
- [11] J. Morillo, J. Usero, D. Rosado, H. El Bakouri, A. Riaza, F.-J. Bernaola, *Desalination* **2014**, 336, 32.
- [12] A. Giwa, V. Dufour, F. Al Marzooqi, M. Al Kaabi, S. W. Hasan, *Desalination* **2017**, 407, 1.
- [13] Y. Shi, C. Zhang, R. Li, S. Zhuo, Y. Jin, L. Shi, S. Hong, J. Chang, C. Ong, P. Wang, *Environ. Sci. Technol.* **2018**, 52, 11822.
- [14] A. K. Menon, I. Haechler, S. Kaur, S. Lubner, R. S. Prasher, *Nat. Sustainability* **2020**, 3, 144.
- [15] A. Al-Karaghoul, L. L. Kazmerski, *Renewable Sustainable Energy Rev.* **2013**, 24, 343.
- [16] M. M. Damtie, R. H. Hailemariam, Y. C. Woo, K. D. Park, J. S. Choi, *Chemosphere* **2019**, 236, 124288.
- [17] N. Ghaffour, T. M. Missimer, G. L. Amy, *Desalination* **2013**, 309, 197.
- [18] A. V. Dudchenko, C. Chen, A. Cardenas, J. Rolf, D. Jassby, *Nat. Nanotechnol.* **2017**, 12, 557.
- [19] A. P. Straub, N. Y. Yip, S. H. Lin, J. Lee, M. Elimelech, *Nat. Energy* **2016**, 1, 16090.
- [20] S. Lin, S. Nejati, C. Boo, Y. Hu, C. O. Osuji, M. Elimelech, *Environ. Sci. Technol. Lett.* **2014**, 1, 443.
- [21] D. M. Warsinger, J. Swaminathan, E. Guillen-Burrieza, H. A. Arafat, J. H. Lienhard, *Desalination* **2015**, 356, 294.
- [22] L. D. Tijjng, Y. C. Woo, J.-S. Choi, S. Lee, S.-H. Kim, H. K. Shon, *J. Membr. Sci.* **2015**, 475, 215.
- [23] S. Meng, Y. Ye, J. Mansouri, V. Chen, *J. Membr. Sci.* **2014**, 463, 102.
- [24] J. Ge, Y. L. Peng, Z. H. Li, P. Chen, S. B. Wang, *Desalination* **2014**, 344, 97.
- [25] M. Sun, C. Boo, W. B. Shi, J. Rolf, E. Shaulsky, W. Cheng, D. L. Plata, J. H. Qu, M. Elimelech, *Adv. Funct. Mater.* **2019**, 29, 1903125.
- [26] C. Liu, J. Lee, J. Ma, M. Elimelech, *Environ. Sci. Technol.* **2017**, 51, 2161.
- [27] C. Liu, A. F. Faria, J. Ma, M. Elimelech, *Environ. Sci. Technol.* **2017**, 51, 182.
- [28] C. Boo, J. Lee, M. Elimelech, *Environ. Sci. Technol.* **2016**, 50, 8112.
- [29] J. Zeng, S. Cui, Q. Wang, R. Chen, *Desalination* **2019**, 459, 105.
- [30] C. Yang, Z. Suo, *Nat. Rev. Mater.* **2018**, 3, 125.
- [31] W. Xie, J. Duan, H. Wang, J. Li, R. Liu, B. Yu, S. Liu, J. Zhou, *J. Mater. Chem. A* **2018**, 6, 24114.
- [32] F. Zhao, X. Zhou, Y. Shi, X. Qian, M. Alexander, X. Zhao, S. Mendez, R. Yang, L. Qu, G. Yu, *Nat. Nanotechnol.* **2018**, 13, 489.
- [33] X. Zhou, F. Zhao, Y. Guo, B. Rosenberger, G. Yu, *Sci. Adv.* **2019**, 5, 5484.
- [34] M. Wallace, D. J. Adams, J. A. Iggo, *Soft Matter* **2013**, 9, 5483.
- [35] W. Zhang, X. Liu, J. Wang, J. Tang, J. Hu, T. Lu, Z. Suo, *Eng. Fract. Mech.* **2018**, 187, 74.
- [36] N. E. Levinger, *Science* **2002**, 298, 1722.

- [37] Y. G. Zheng, H. F. Ye, Z. Q. Zhang, H. W. Zhang, *Phys. Chem. Chem. Phys.* **2012**, *14*, 964.
- [38] A. Faraone, L. Liu, C. Y. Mou, C. W. Yen, S. H. Chen, *J. Chem. Phys.* **2004**, *121*, 10843.
- [39] B. Amsden, *Macromolecules* **1998**, *31*, 8382.
- [40] J. Zeng, Q. Y. Wang, Y. Shi, P. Liu, R. K. Chen, *Adv. Energy Mater.* **2019**, *9*, 1900552.
- [41] A. Deshmukh, M. Elimelech, *J. Membr. Sci.* **2017**, *539*, 458.
- [42] R. M. Venable, A. Kramer, R. W. Pastor, *Chem. Rev.* **2019**, *119*, 5954.
- [43] C. Yan, P. L. Kramer, R. Yuan, M. D. Fayer, *J. Am. Chem. Soc.* **2018**, *140*, 9466.
- [44] H. Ju, A. C. Sagle, B. D. Freeman, J. I. Mardel, A. J. Hill, *J. Membr. Sci.* **2010**, *358*, 131.
- [45] G. Hoch, A. Chauhan, C. J. Radke, *J. Membr. Sci.* **2003**, *214*, 199.
- [46] J. Duan, W. Xie, P. Yang, J. Li, G. Xue, Q. Chen, B. Yu, R. Liu, J. Zhou, *Nano Energy* **2018**, *48*, 569.
- [47] J. Zhang, Z. Y. Song, B. A. Li, Q. Wang, S. C. Wang, *Desalination* **2013**, *324*, 1.
- [48] Y. Guo, F. Zhao, X. Zhou, Z. Chen, G. Yu, *Nano Lett.* **2019**, *19*, 2530.